ELSEVIER

Thin Solid Films 302 (1997) 127–132

thin solid films

Morphology of $TiSi_2$ films on Si formed from co-deposited Ti and Si

S.B. Herner [a,1], V. Krishnamoorthy [a], A. Naman [a], K.S. Jones [a], H.-J. Gossmann [b], R.T. Tung [b]

[a] *Department of Materials Science and Engineering, University of Florida, Gainesville, FL 32611, USA*
[b] *Bell Laboratories, Lucent Technologies, Murray Hill, NJ 07974, USA*

Received 11 September 1996; accepted 5 December 1996

Abstract

Titanium disilicide ($TiSi_2$) films formed from varying compositions of co-deposited Ti and Si on a Si substrate and annealed in argon at 850°C have been characterized by Rutherford backscattering, Auger electron spectroscopy, transmission electron microscopy, atomic force microscopy, and high resolution X-ray diffraction. As-deposited films ($TiSi_x$) with $x < 2$ form a TiO_xN_{1-x} film on top of a $TiSi_2$ film after annealing, while "Si-rich" ($x > 2$) film form $TiSi_2$ with a poly Si film on top. This result is explained by the strong driving force of Ti to form an oxide or nitride with ambient gases while Si must diffuse through the growing film to form $TiSi_2$. An "Si-rich" as-deposited composition ($x > 2$) results in less interface roughening between the $TiSi_2$ film and Si substrate after annealing, as well as greater residual wafer curvature as compared to the other samples. The reduced wafer curvatures in the "Si-deficient" samples is attributed to the presence of the TiO_xN_{1-x} film which acts to counter the stress in the $TiSi_2$ film. © 1997 Elsevier Science S.A.

Keywords: Silicides; Transmission electron microscopy (TEM)

1. Introduction

The widespread use of C54 phase $TiSi_2$ as an ohmic contact in Si and the drive toward lower processing temperatures has led to heightened interest in the reaction products and morphology of $TiSi_2$ films on Si. Titanium disilicide has low resistivity, high temperature stability, resistance to electromigration, and the ability to self-align in CMOS transistors [1]. Titanium nitride (TiN) is often used as a diffusion barrier between $TiSi_2$ contacts and the interconnect material. Conditions that produce both $TiSi_2$ and TiN films have therefore been scrutinized closely [2,3]. The severe roughening that can occur at the $TiSi_2$/Si interface can degrade device performance and is therefore also of interest [1]. Other investigators have found that $TiSi_2$ formation can be influenced by ion implantation of the substrate [4,5], by the annealing ambient [6], and by the nature of the substrate (i.e. single crystal, polycrystalline, or amorphous) [7,8]. Alternate methods of depositing $TiSi_2$, such as CVD, have achieved selective deposition with minimal Si consumption [9].

Herner et al. [10] have recently investigated and reported on the native point defect perturbance in Si caused by the presence of $TiSi_2$ films formed from co-deposited Ti and Si. In this paper we report on the microstructure of these films, which were formed on single crystal, unimplanted Cz–Si. Annealing of Ti or Ti + Si films in argon resulted in a bi-layer structure: TiO_xN_{1-x} on top and C54 $TiSi_2$ underneath. The formation of the TiO_xN_{1-x} film can be suppressed by the co-deposition of "excess" Si ($TiSi_x$ with $x > 2$). This "excess" Si also reduces the grain size of the resulting $TiSi_2$ film, which reduces the interface roughening between the $TiSi_2$ film and Si substrate but also increases the residual stress in the film after annealing.

2. Experimental

All samples were prepared from the same 50 mm Si (100) float zone grown wafer ($\rho > 1000\ \Omega$m). The wafer was diced into three samples 15 × 20 mm. Prior to metal deposition, all samples were cleaned by a dilute HF (1:20) dip. The samples were loaded into an ultra-high vacuum MBE chamber that was pumped down to a base pressure

[1] Now with Bell Laboratories, Lucent Technologies, Murray Hill, NJ 07940, USA.

PII S0040-6090(96)09586-7

of 1×10^{-10} Torr. For each sample, Ti of 99.995% purity and Si were co-evaporated by electron beam in appropriate amounts. Rutherford backscattering spectrometry (RBS) was performed on the as-deposited samples using 2 MeV He^+ ions and scattering angles of 98° and 172°. The samples were rotated during backscattering to prevent channeling. Backscattered spectra were analyzed using the RUMP software program [11]. The samples were placed in a tube furnace that was pumped down to a vacuum better than 10^{-7} Torr. Argon of 99.995% purity was then admitted to the furnace. Impurities in the argon were estimated by the manufacturer to be < 25 ppm N_2, < 8 ppm O_2, < 2 ppm H_2O, and < 1 ppm hydrocarbons. Before furnace entry, the gas was first passed through a copper coil cooled by a mixture of dry ice and acetone to prevent H_2O intrusion. The samples were annealed for 60 minutes at 850 °C.

X-ray rocking curves from the annealed samples were obtained from a Philips HR-1 X-ray diffractometer with a Bonse–Hart collimator and a Bartles monochromator. Samples were mounted in the X-ray system using beeswax to minimize any strain induced from mounting. After optimizing specimen tilt and rotation for maximum intensity, the samples were "rocked" through the (400) Bragg angle reflection at several locations on the same sample. The change in peak position as a function of sample translation was then used to evaluate wafer curvature. Derivation of the wafer curvature from this peak shift is described in greater detail in [12]. Auger electron spectroscopy (AES) was performed using a Perkin Elmer Phi 660 scanning Auger microprobe. The films were sputtered with a 3 keV Ar^+ beam at 100 nA at 30° angle of incidence, through a 3×3 mm crater. A 5 keV electron beam was rastered over an area of 20×20 μm in the center of the crater. The electron beam current was 5 nA and the angle of incidence 30°. Transmission electron microscopy (TEM) was performed with a JEOL 200CX operating at 200 keV. Cross-sectional (XTEM) samples were prepared by standard dicing, lapping, and ion milling techniques. Plan view (PTEM) samples were prepared by lapping and chemically etching from the backside with an $HF:HNO_3$ solution (1:3). Specimens were imaged in bright field mode. Atomic force microscopy (AFM) was performed using a Digital Instruments Nanoscope III. The silicide film was removed from the samples by chemically etching in a dilute HF (25%) solution for 6 minutes. The underlying Si surface was then profiled using tapping mode with a resolution of 0.01 nm.

3. Results

3.1. As-deposited compositions and densities

Films were deposited with the nominal compositions Ti, TiSi, and $TiSi_{2.5}$, in three separate samples, respectively.

Table 1
As-deposited compositions measured by ion scattering

Sample	Ti ($\times 10^{17}$ atoms cm^{-2})	Si ($\times 10^{17}$ atoms cm^{-2})
Ti (only)	1.1	–
$TiSi_{0.8}$	1.2	0.98
$TiSi_{2.2}$	1.3	2.7
Volume density ($\times 10^{22}$ atoms/cm^3)	5.7	5.0

The mass deposition conditions and flux were tailored to deposit the same total number of Ti atoms per unit area on each sample. Ion backscattering was used to measure the areal atomic densities and determine the actual as-deposited compositions, which are listed in Table 1. Using the atomic density of Ti, the Ti (only) film should have a thickness of 22 nm, as derived from backscattering data. A direct measurement of the film thickness via XTEM (Fig. 1) on the as-deposited Ti (only) sample yields 30 nm. The as-deposited thicknesses were 70 nm ($TiSi_{0.8}$) and 90 nm ($TiSi_{2.2}$), as measured by XTEM on the other samples. Using the volume atomic density of Ti and Si, the measured area densities, and a rule of mixtures approximation for the compositions, we derive calculated thicknesses of 41 nm ($TiSi_{0.8}$) and 78 nm ($TiSi_{2.2}$). These measurements show the as-deposited films are porous.

The as-deposited films show a columnar structure typical of deposited metal films (Fig. 1) [13]. This same structure was representative of all three samples. Jeon et al. [6] have speculated that interface roughening between the $TiSi_2$ and Si originates from Si selectively diffusing into this grain structure. However, the size of the roughness (peak-to-valley) is much larger than the diameter of these columnar grains, indicating that this is not the origin of the roughening.

3.2. AES analysis of the annealed films

Fig. 2 shows the Auger spectrum from the annealed $TiSi_{0.8}$ sample, also representative of the spectrum from the annealed Ti (only) sample. Overlap between the Ti (LMM) and N (KVV) lines prevented Ti and N data to be profiled concurrently, so that we choose to follow Ti [2]. However, sputtering was halted several times to allow for a more accurate check by a three point method for the

Fig. 1. XTEM micrograph of the Ti film, as-deposited.

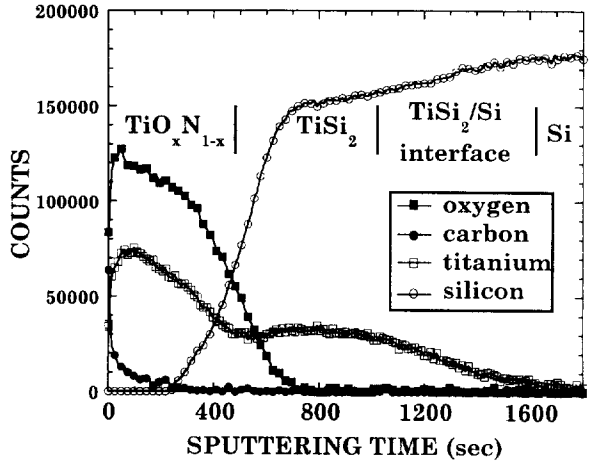

Fig. 2. Auger spectra from the annealed $TiSi_{0.8}$ sample.

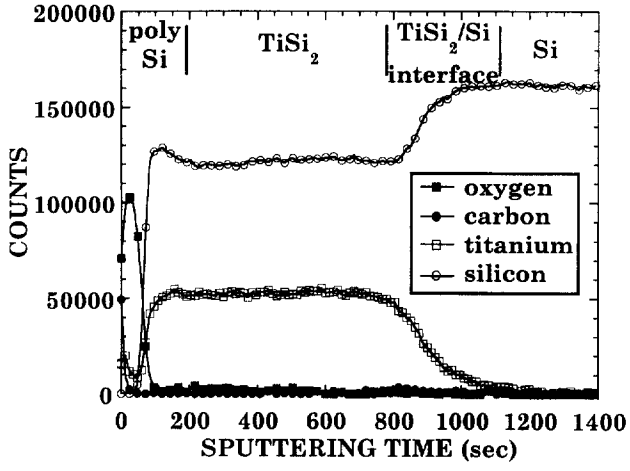

Fig. 3. Auger spectra from the annealed $TiSi_{2.2}$ sample.

presence of N. Nitrogen's presence was found to coincide with that of oxygen. Due to the differing Auger sensitivity of the elements, changes in the Auger sensitivity of the elements with TiO_xN_{1-x}, $TiSi_2$, and Si, and preferential sputtering, the peak counts of the Auger electrons of the differing elements could not be used to determine the compositions of the individual films. The TiO_xN_{1-x} film can clearly be seen in the spectra, along with the $TiSi_2$ layer. The rough $TiSi_2$/Si interface is evident in the slow decay of the Ti signal and slow increase in the Si signal at about 1000 seconds into the sputtering in Fig. 2.

The AES spectrum from the annealed $TiSi_{2.2}$ sample is shown in Fig. 3. It confirms that little, if any, TiO_xN_{1-x} formed on top of the $TiSi_2$ in this sample. It also indicates that at least some of the "excess" deposited Si lies on top of the $TiSi_2$ film. A quantification of how much of the "excess" Si exists on top of the $TiSi_2$ film is not possible. The relatively steeper decay in the Ti signal and steeper increase in the Si signal indicate the interface was not as rough as in the other two samples, as was confirmed by AFM (to be discussed).

3.3. XTEM of the annealed films

Representative cross-sections of each of the three films after annealing are shown in Fig. 4. All the samples show severe roughening at the $TiSi_2$/Si interface. The annealed Ti (only) and $TiSi_{0.8}$ samples both show a distinct bi-layer film formation. The top film was shown by AES and electron diffraction to be TiO_xN_{1-x} (cubic), while the bottom film was C54 $TiSi_2$. Despite being annealed in 99.995% pure argon, Ti's strong affinity for O and N led to the bi-layer structure [3]. The annealed $TiSi_{2.2}$ film XTEM micrograph does not distinctly show a bi-layer structure. However, the AES spectrum and PTEM micrograph (to be discussed later) for this sample definitively

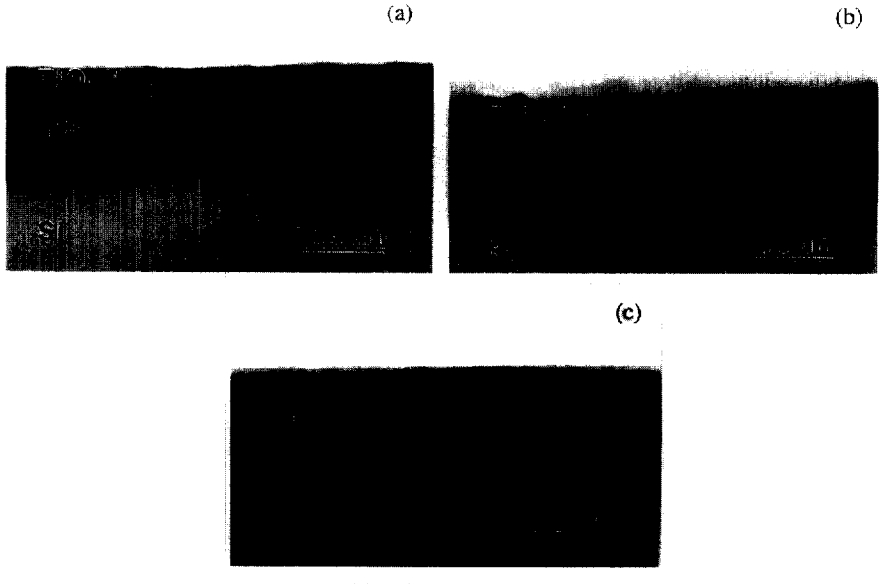

Fig. 4. XTEM micrograph of the annealed (a) Ti (only) sample, (b) $TiSi_{0.8}$ sample, and (c) $TiSi_{2.2}$ sample.

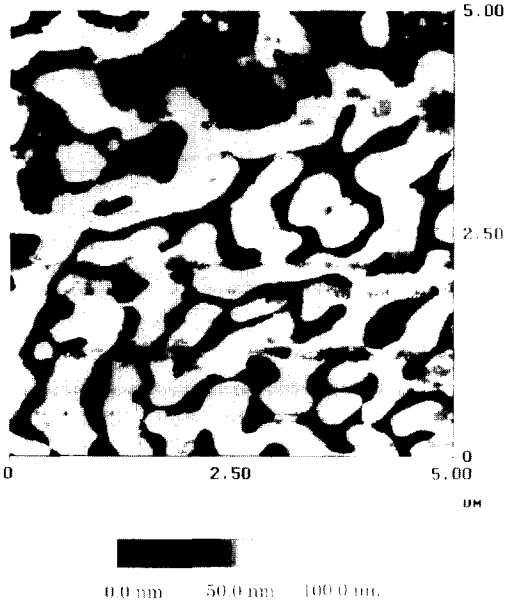

Fig. 5. Representative AFM micrograph of the underlying Si surface of Ti (only) sample after annealing and chemically etching off the films.

show a poly Si film on the surface. This indicates that either the poly Si is very thin or discontinuous, or both. Silicide thicknesses for the annealed films could not be accurately measured because of the extreme roughness at the interface. By using the amount of Ti deposited, we can calculate how much $TiSi_2$ should form based on the data from Murarka [14]. The sample with Ti (only) should produce a $TiSi_2$ thickness of 55 nm, while the co-deposited samples should produce 62 nm ($TiSi_{0.8}$) and 70 nm ($TiSi_{2.2}$). Some of the Ti is consumed in the TiO_xN_{1-x} film in the Ti and $TiSi_{0.8}$ samples, reducing the amount available to form $TiSi_2$.

3.4. Interface roughness

Atomic force microscopy showed that the $TiSi_2$ films from the annealed Ti (only) and $TiSi_{0.8}$ samples have approximately the same degree of roughening at the $TiSi_2$/Si interface, confirming the XTEM and AES observations. A representative plot of the underlying Si surface from the annealed Ti (only) sample (Fig. 5) shows the characteristic shape caused by grain boundary roughening [15]. The annealed $TiSi_{2.2}$ sample showed reduced roughening at the interface as compared to the other samples (Table 2).

Table 2
Root mean square roughnesses of the $TiSi_2$/Si interface for the samples after annealing

Composition before annealing	$TiSi_2$/Si roughness after annealing (nm)
Ti	30.0
$TiSi_{0.8}$	27.2
$TiSi_{2.2}$	8.3

3.5. Plan view TEM

The grain sizes of the films were measured by plan view TEM. Fig. 6 shows the grain structure of the films in the annealed Ti (only) sample. The TiO_xN_{1-x} film has a fine, equi-axed grain structure with grain sizes on the order of 10–40 nm (Fig. 6(a)). The $TiSi_2$ grains are elongated platelets, and are approximately 200–500 nm in size (Fig. 6(b)). The $TiSi_2$ grains from the annealed $TiSi_{0.8}$ sample had a similar microstructure and size after annealing. The poly Si film on the annealed $TiSi_{2.2}$ film was revealed by PTEM (Fig. 7(a)), and the grains are on the order of 20–30 nm. The $TiSi_2$ grains from the annealed $TiSi_{2.2}$ sample (Fig. 7(b)) were somewhat larger in size (200–1000 nm) compared to the other samples, but have the same elongated platelet structure. Note the presence of twins within the $TiSi_2$ grains in both micrographs. By etching from the backside of the wafer, we are able to image both the TiO_xN_{1-x} or poly Si film and the $TiSi_2$ film (Fig. 8). The $TiSi_2$ grain size comes from area 1 while the TiO_xN_{1-x} or poly Si image comes from area 2.

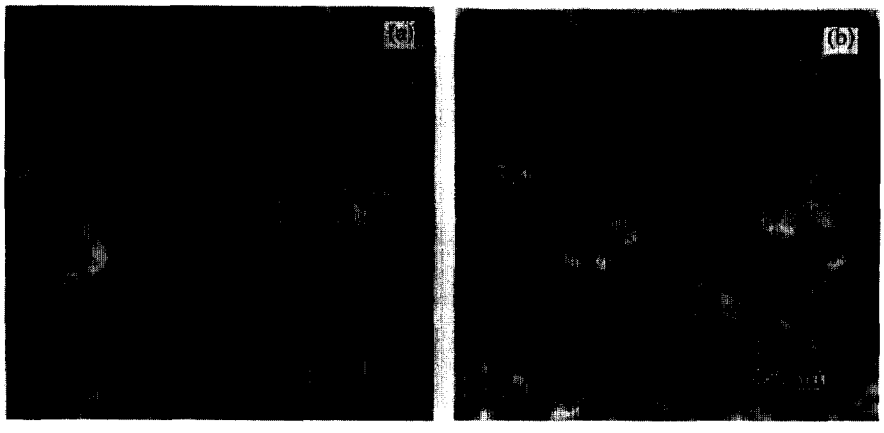

Fig. 6. PTEM micrographs of the (a) TiO_xN_{1-x} film on top of the $TiSi_2$ film, and (b) $TiSi_2$ film (the annealed Ti (only) sample was imaged).

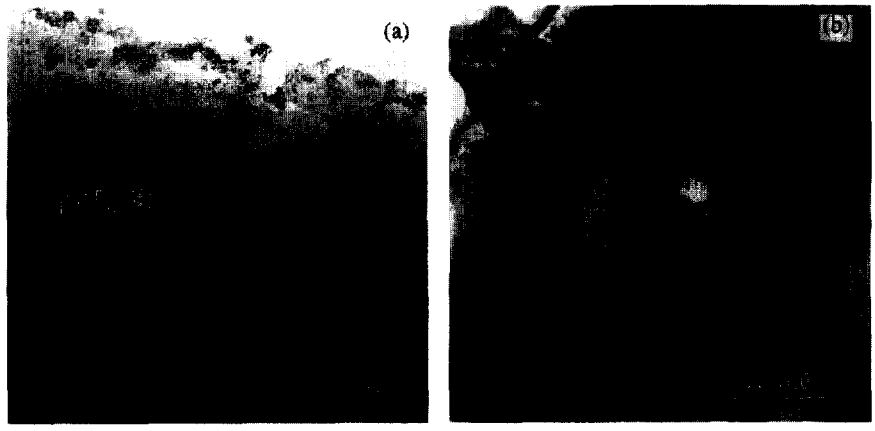

Fig. 7. PTEM micrographs of the (a) poly Si film on top of the $TiSi_2$ film, and (b) $TiSi_2$ film (the annealed $TiSi_{2.2}$ sample was imaged).

3.6. Residual wafer flexure

Through the technique described in [12], we are able to determine the residual wafer flexure in the samples after annealing. Table 3 shows the measured sample curvatures from the three samples. The two samples with $x < 2$ ($TiSi_x$) show a larger residual sample curvature, indicating that the substrate has a small residual stress, while the Si-rich ($x > 2$) composition has a smaller residual radius of curvature indicating larger stress in the substrate.

4. Discussion

Only the "Si-deficient" ($x < 2$) compositions formed a top film of TiO_xN_{1-x} but not the "Si-rich" ($x > 2$) composition. We explain this difference by the need for Si to diffuse across the growing silicide film to form $TiSi_2$ [16], allowing time for the competing Ti + O + N = TiO_xN_{1-x} reaction to occur in the Ti and $TiSi_{0.8}$ (as-deposited) samples. The "Si-rich" sample (as-deposited) had only to crystallize into the C54 $TiSi_2$ phase with minimal diffusion distances for Si.

Our observation that the surface film is TiO_xN_{1-x} and not TiN is based on the AES profiles and electron diffraction data. Oxygen was prevalent throughout the top film and had not, therefore, been "snowplowed" to the interface [17]. Electron diffraction showed the film has the cubic structure of TiN, indicating but not proving O is substituting on N sites. It is possible that O is present in some other form, such as TiO_2, in such small amounts that it is not detected by electron diffraction while it does show in the AES analysis. Morgan et al. [2] also found that TiO_xN_{1-x} forms on top of C54 $TiSi_2$ when the film is annealed above 800 °C, sometimes with a small amount of Si on top of the oxynitride. The composition and origin of the film on top of the silicide is of some debate [2,3,17]. While titanium oxides are generally more thermodynamically stable than titanium nitrides, a diffusion limited reaction may be occurring, in which the larger concentration of N enables the oxynitride to form instead of a pure oxide. Further experimentation is needed on the composition and structure of the oxynitride.

The film on top of the $TiSi_2$ film in the annealed $TiSi_{2.2}$ sample is identified as poly Si, based on the AES profile and the grain structure (Fig. 7a). This finding shows that at least some of the "excess" Si has diffused to the free surface of the $TiSi_2$ film. Our previous study has shown that this sample does not result in a larger supersaturation of vacancies in the Si substrate than in the other samples [10]. Honeycutt et al. [18] speculated that Si diffusing across the grain boundaries of $TiSi_2$ films can be responsible for a continued vacancy injection into the substrate, which these results, along with the earlier reported results [10], contradict. No real difference was seen in the native point defect behavior in the underlying Si despite the large difference in grain sizes of the films [10].

The reduced interface roughening in the annealed $TiSi_{2.2}$ sample cannot be explained by the difference in grain size in this sample as compared to the others. Indeed, we would

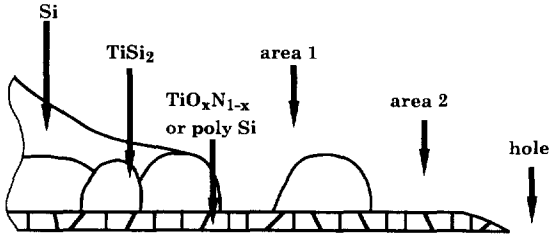

Fig. 8. Schematic cross-section of the PTEM samples.

Table 3
Radii of curvature for the samples after annealing

Composition before annealing	Sample curvature after annealing (m)
Ti	53.4
$TiSi_{0.8}$	238.3
$TiSi_{2.2}$	30.9

expect that a larger grain size would produce more severe roughening, as interface roughening is due to faceting of the grains to lower the overall surface energy of the film [15]. We can only speculate as to why the $TiSi_2$ grains in the "Si-rich" sample after annealing are larger than in the other samples: it is possible that grain growth may have been more rapid in this sample due to the readily available Si or that the TiO_xN_{1-x} layer in the other samples acts to somehow retard grain growth. Since some Ti is consumed in the TiO_xN_{1-x} film, the $TiSi_{2.2}$ (as-deposited) sample has a thicker $TiSi_2$ film after annealing, which encourages the growth of larger grains, but this cannot account for all of the size difference.

Svilan et al. [19] have shown that $TiSi_2$ formation results in a residual tensile stress after annealing. All of our samples showed a positive residual tensile stress in the film. The difference in sample curvature is in rough agreement with a previous study by Murarka and Fraser [20]. Murarka and Fraser showed that "excess" Si deposited with Ti leads to less tensile stress when the phase changes from Ti + Si to $TiSi_2$. They speculated that as the amount of "excess" Si reached a critical value, Si interstitials in the $TiSi_2$ lattice create a compressive stress. Since Murarka and Fraser determined the Si:Ti ratio by sputtering parameters, which we have found to be inaccurate for composition determination, the actual composition of their samples may have been different from what was reported [20]. Since no experimental determination of the amount of strain that an Si interstitial exerts on the $TiSi_2$ lattice has been made, we cannot a priori rule out this theory. However, it is doubtful that the C54 structure of $TiSi_2$ would permit enough interstitials to account for the reduced curvature. Shor and Pelleg [21] postulated that a TiO_xN_{1-x} film acts to counteract the residual stress of the $TiSi_2$ film, which this work supports. Based on the observations, we believe the high degree of curvature observed in the substrate of the annealed $TiSi_{2.2}$ sample is due to the absence of a TiO_xN_{1-x} film.

5. Conclusion

Co-deposition of Si and Ti on Si with $x < 2$ ($TiSi_x$) results in the formation of a bi-layer structure when annealed in argon at 850°C: a TiO_xN_{1-x} film on top of a $TiSi_2$ (C54) film. The co-deposition of Si with $x > 2$ suppresses the formation of a TiO_xN_{1-x} film, results in a somewhat larger grain size in the $TiSi_2$ film, and reduces the $TiSi_2$/Si interface roughening as compared to samples with $x < 2$. At least some of the excess Si in the $x > 2$ sample (as-deposited) has diffused to the free surface, forming a poly Si film. Furthermore, the residual tensile stress after annealing in the sample with $x > 2$ is much greater due to the absence of the TiO_xN_{1-x} film.

Acknowledgements

The authors would like to thank Eric Lambers for help with the Auger profiling. The work at the University of Florida was supported by a grant from SEMATECH. One of the authors (SBH) would like to thank Bell Laboratories, Lucent Technologies, for partial financial support.

References

[1] K. Maex, Mat. Sci. Eng. Rep. R11 (1993) 53.
[2] A.E. Morgan, E.K. Broadbent, A.H. Reader, Mat. Res. Soc. Sym. Proc. 52 (1986) 279.
[3] S.B. Desu, J.A. Taylor, J. Am. Ceram. Soc. 73 (1990) 509.
[4] W. Lur, L.J. Chen, J. Appl. Phys. 66 (1989) 3604.
[5] M.H. Wang, W. Lur, H.C. Cheng, L.J. Chen, Mat. Res. Soc. Sym. Proc. 100 (1988) 93.
[6] H. Jeon, C.A. Sukow, J.W. Honeycutt, G.A. Rozgonyi, R.J. Nemanich, J. Appl. Phys. 71 (1992) 4269.
[7] Q.Z. Hong, S.Q. Hong, F.M. D'Heurle, J.M.E. Harper, Thin Solid Films 253 (1994) 279.
[8] R.T. Tung, Appl. Phys. Lett. 68 (1996) 1933.
[9] R. Madar, C. Bernard, Appl. Surf. Sci. 53 (1991) 1.
[10] S.B. Herner, K.S. Jones, H.-J. Gossmann, R.T. Tung, J.M. Poate, H.S. Luftman, Appl. Phys. Lett. 68 (1996) 3870.
[11] L. Doolittle, M. Thompson, RUMP Users Manual, Cornell University, Ithaca, NY, 1985–1994.
[12] Philips High Resolution Diffractometer Instruction Manual, 2nd ed., Eindhoven, Netherlands, 1989.
[13] R. Messier, J. Vac. Sci. Tech. A 4 (1986) 490.
[14] S.P. Murarka, Silicides for VLSI Applications, Academic Press, New York, 1983.
[15] C.A. Sukow, R.J. Nemanich, J. Mat. Res. 9 (1994) 1214.
[16] W.K. Chu, S.S. Lau, J.W. Mayer, H. Muller, K.N. Tu, Thin Solid Films 25 (1975) 393.
[17] J.F. Jongste, F.E. Prins, G.C.A.M. Janssen, S. Radelaar, Appl. Surf. Sci. 38 (1989) 57.
[18] J.W. Honeycutt, J. Ravi, G.A. Rozgonyi, Mat. Res. Soc. Sym. Proc. 262 (1992) 701.
[19] V. Svilan, J.M.E. Harper, C. Cabral Jr., L.A. Clevenger, Mat. Res. Soc. Sym. Proc., to be published.
[20] S.P. Murarka, D.B. Fraser, J. Appl. Phys. 51 (1980) 350.
[21] Y. Shor, J. Pelleg, Mat. Res. Soc. Sym. Proc. 402 (1996) 107.